Experimental and Theoretical Study of the Metallotropic Migrations in Cyclooctatetraeneosmiumtricarbonyl

Ilya D. Gridnev,* Nurbosyn U. Zhanpeisov,* and Mia Karenina C. del Rosario

Department of Chemistry, Graduate School of Science, Tohoku University, Aoba, Sendai, 980-8578, Japan

Received: January 31, 2005; In Final Form: April 26, 2005

Experimental verification of the mechanism of metallotropic migrations in cyclooctatetraeneosmiumtricarbonyl (**3**) by means of 2D EXSY NMR spectroscopy confirmed the mechanism of [1,2]-Os shifts with low activation barrier ($E_A = 5.9 \pm 0.2$ kcal mol^{-1}, $\ln A = 32 \pm 1$). Transition-state structure for this rearrangement obtained at the B3LYP/SDD level of theory testifies for the activation energy of 6.5 kcal mol^{-1} and supports well the selective [1,2]-Os shifts observed for **3**.

Introduction

Metallotropic rearrangements belong to an important type of electronically controlled intramolecular reactions with minimized importance of the solvent effects or of any other intermolecular interactions. A simple theoretical basis for the sigmatropic rearrangements of the type has been created within the orbital symmetry conservation principle,[1] whereas recent studies demonstrated how the frontier orbital approach can be applied to analysis of sigmatropic migrations in cyclic polyenes.[2] However, haptotropic migrations of organometallic groups across the π-systems of polyenic cycles have been so far only scarcely studied theoretically, whereas the experimental data are extensive but nonsystematic. Theoretical analysis of such rearrangements is complicated because of complexity of domains and channels at the potential energy surface as well as because of lack of well-established approaches in such kind of theoretical studies.

Experimental determination of the mode of metallotropic migrations in cyclooctatetraene (COT) derivatives of iron and ruthenium has been one of the most challenging problems in the early stage of the studies of metallotropic rearrangements.[3] Several research groups have attempted to use the direct line-shape analysis of the temperature-dependent NMR spectra of the complexes **1**−**2**[4,5] shown in Scheme 1. The careful and extensive analysis of the experimental and computed line shapes suggested that the most probable mechanism of the fast metallotropic migrations are consecutive and random [1,2]-M shifts.[5] However, the technical limitations of those days and inevitably qualitative character of the conclusions had not allowed to be completely certain in the uniqueness of the [1,2]-M migration mechanism, while the kinetic estimations were unreliable. The osmium compound **3** (Scheme 1) has been a subject of a single study[6] demonstrating a higher barrier for metallotropic migrations compared to similar rearrangements in **1** and **2**. Nevertheless, even in this relatively favorable case (the corresponding NMR spectra could be obtained at −100 °C), the line-shape analysis provided only qualitative estimation of the migration mechanism, whereas the kinetic analysis has not been attempted.[6] Moreover, to the best of our knowledge, we are not aware of any theoretical paper in the literature devoted to considerations of these metallotropic intramolecular transformations.

SCHEME 1: COT Derivatives with Different Metals of Me: 1, Fe; 2, Ru; 3, Os

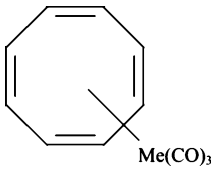

We report here the results of experimental and theoretical studies on the mechanism of haptotropic migrations in the osmiumtricarbonyl (OTC) complex of cyclooctatetraene **3** using modern 2D NMR techniques and highly popular DFT computations. The osmium compound has been chosen because of its relatively slow rearrangement rate as compared to the iron and ruthenium compounds making possible to get the unambiguous signal assignment in the NMR spectra at −100 °C.

Experimental Section and Calculation Method

All experiments were performed under dry argon atmosphere. ^{1}H and ^{13}C NMR spectra of **3** were recorded using a JEOL AL-300 spectrometer. ^{1}H 2D EXSY NMR spectra were acquired in the phase-sensitive mode using the States−Haberkorn−Ruben method.[7] Areas of cross-peaks and diagonal peaks were obtained by volume integration of appropriate voxels surrounding the peaks. They were determined after phase and baseline correction in both dimensions using the JEOL Delta software. The temperature controller of the spectrometer was calibrated with the standard sample containing 4% of methanol in methanol-d_4 from Bruker.

Rate constants at each temperature were derived from the experimental intensities via exchange matrix resolution approach[8] using MestRec EXSYCalc software.[9] The activation parameters of a rearrangement were derived via averaging the six values arising from the same exchange process. The determination of a rate constant at each temperature required two experiments, that is, one with higher mixing times of 10−1000 ms (optimized to find the value that gives the cross-peaks with higher intensity) for the exchange experiment while the other one with lower mixing times of 0.01 ms to determine the volumes of an autopeak in the nonexchange spectra. At 193 K,

* Address correspondence to these authors. E-mail: nurbosyn@orgphys.chem.tohoku.ac.jp.

10.1021/jp050526b CCC: $30.25
Published on Web 06/03/2005

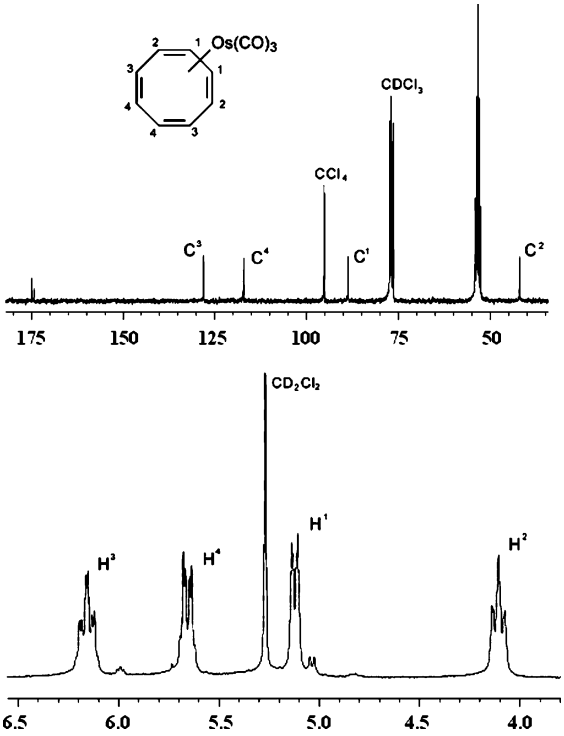

Figure 1. ^{1}H NMR (below, 300 MHz, −100 °C, CD_2Cl_2−$CDCl_3$−CCl_4 mixture) and ^{13}C NMR (above, 75 MHz, −100 °C, CD_2Cl_2−$CDCl_3$−CCl_4 mixture) spectra of **3**.

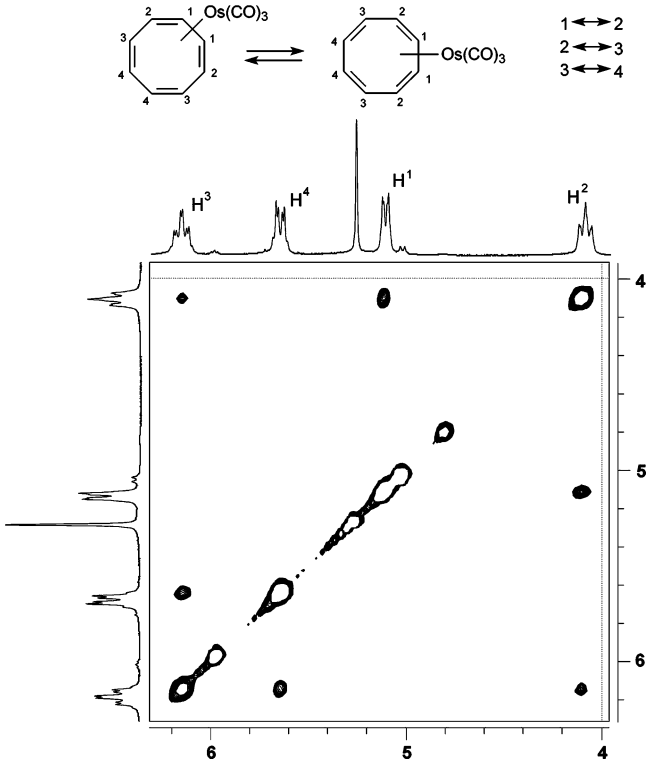

Figure 2. Phase-sensitive ^{1}H−^{1}H 2D NMR EXSY spectrum (300 MHz, −100 °C, CD_2Cl_2−$CDCl_3$−CCl_4 mixture, mixing time 50 ms) of **3**.

experiments with the mixing times of 0.01, 10, 20, 30, 40, 50 and 60 ms were performed. Moreover, the rate constant thus derived was additionally checked by the complimentary so-called initial rate method[10] that shows a good coincidence of the results obtained by both techniques.

DFT calculations were performed with the use of Becke's three-parameter hybrid method with the Lee, Yang, and Parr (B3LYP) gradient-corrected correlation functional.[11] Geometry optimizations were carried out using the standard SDD basis sets (i.e., Stuttgart/Dresden basis sets with effective core potentials) and Gaussian98 program packages.[12] The minimum energy or transition-state structures were further verified by performing frequency calculations and analyzing the energy second derivatives.

Results and Discussion

Experimental Determination of the Topology and Kinetics of the Rearrangement. Figure 1 displays the ^{1}H and ^{13}C NMR spectra of **3** taken at −100 °C. The assignment of the signals in the spectra has been made by standard 2D correlation techniques. Observation of four signals in ^{1}H and ^{13}C NMR corresponds to the frozen structure of the complex **3**. Moreover, the carbonyl signal in the ^{13}C NMR spectrum is split into two resonances with intensity ratio of 2:1 which indicates the fact that the rotation of the OTC group is also frozen.

Each of the possible mechanisms for the OTC group migrations results in unique combination of the exchanging protons (or carbon atoms) in different possible metallotropic rearrangements of **3** as is illustrated in Scheme 2. Therefore, the 2D EXSY NMR experiments would be the most straightforward way to determine the topology of the migration of OTC groups. The mechanism of metallotropic rearrangements occurring in **3** directly follows from the ^{1}H−^{1}H EXSY spectra taken in the temperature interval 173−198 K (e.g., see, Figure 2). The spectrum unequivocally attests for the [1,2]-Os migrations without any appreciable interference of other mechanisms. At higher temperatures and longer mixing times, all possible cross-peaks are observed in the EXSY spectra. However, these are caused by the several consecutive [1,2]-migrations that have been verified by checking the dependence of the relative volumes of corresponding cross-peaks against mixing time in a series of the EXSY spectra taken at 198 K with mixing times varying from 10 to 50 ms. Rate constants for the [1,2]-Os migrations were obtained by volume integration of the cross-peaks in the EXSY spectra followed by transformation of the intensity matrix to the rate matrix.[8,9] Figure 3 displays the Arrhenius plot attesting for the following activation parameters: E_A=5.9 ± 0.2 kcal mol^{-1}, ln A = 32 ± 1.

SCHEME 2: Analysis of the Exchanging Atoms in Different Possible Metallotropic Rearrangements of 3

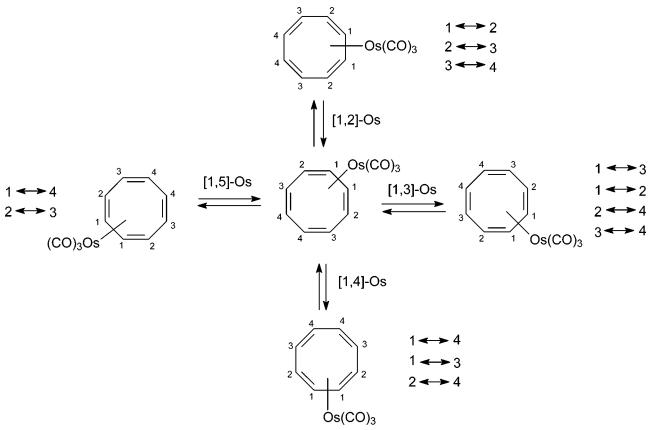

Theoretical DFT Calculations of the Rearrangement. According to the recent paper of Zewail and co-workers[13] as well as other previous experimental and theoretical investigations,[14−16] COT has a tub-shaped (D_{2d}) structure in the electronic ground state while its monoanion has a planar (D_{4h})

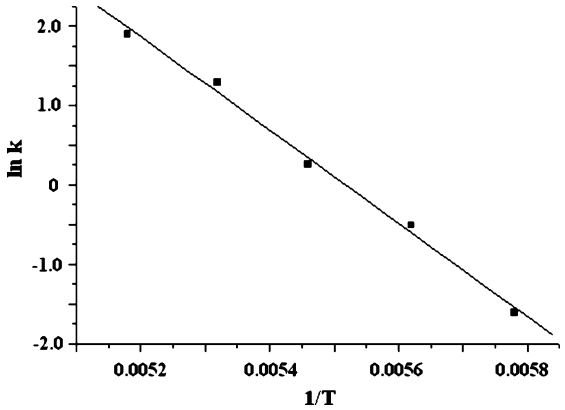

Figure 3. Arrhenius plot for the [1,2]-Os shift in **3**.

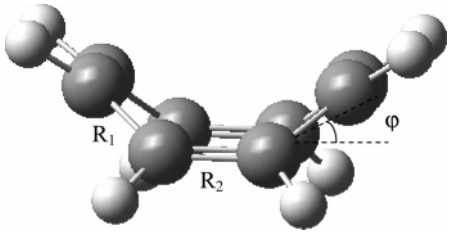

Figure 4. The definition of structural parameters for the considered four structures of COT listed in Table 1. Note that **4** and **5** correspond to minimum structures while **6** and **7** are transition-state structures, respectively.

TABLE 1: Relative Energy (ΔE, kcal mol^{-1}), Symmetry, Geometry (R_1 and R_2, Å; Tub-Shaped Angle φ, Degree), and Mulliken Charges (Q_{C1}, Q_{C2}, Q_{H1}, Q_{H2}, All in e$^-$) for COT Estimated at B3LYP/SDD Level[a]

	structure			
property	**4**	**5**	**6**[b]	**7**
ΔE[c]	0	+28.9	+8.9	+10.0
symmetry	D_{2d}	C_{2h}	C_s	D_{4h}
R_1	1.357	1.418	1.360	1.365
R_2	1.483	1.418	1.485	1.477
φ	39	0	0	0
Q_{C1}	−0.19	−0.01	−0.18	−0.18
Q_{C2}	−0.19	−0.35	−0.18	−0.18
Q_{H1}	0.19	0.17	0.18	0.18
Q_{H2}	0.19	0.19	0.18	0.18

[a] For the definition of selected distances and atoms, see Figure 4. C1 and C2 are the next-nearest-neighbor carbon atoms of the ring while H1 and H2 are bonded to these explicit C atoms. [b] The values of charges differ at the third decimal positions for **6** and **7**. [c] The total energy of **4** is taken as a reference. It equals −309.53462 au.

structure that resembles the geometry of neutral COT at the transition state of the ring inversion. Taking these data into account, we have first considered potential structures for COT, the optimized structures of which are shown in Figure 4 while some of their estimated properties are listed in Table 1. It was found that among the considered four structures, D_{2d} symmetry structure **4** (Figure 4) is indeed global minimum on the potential energy surface while another minimum energy structure **5** with C_{2h} symmetry lies higher for 29 kcal mol^{-1}. The angle φ of the tub-shaped structure **4** is estimated to be 39°. Frequency calculations have shown lack of the presence of any imaginary frequencies in both **4** and **5**. Also, **5** is the only structure where one may observe a strong alternation in the charge distribution among C atoms (as a consequence of this, also among the H atoms) of the eight-member ring while for the other three structures the difference in charge distributions is negligibly small (see Table 1). This observation for **5** is quite interesting

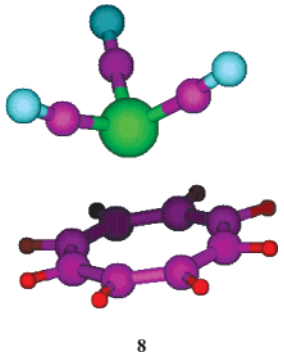

8

Figure 5. The optimized structure of TCO with **5** at the highest spin state. Osmium atom establishes eight Os−C bonds with the ring's carbon atoms at distances ranging from 3.413 to 3.477 Å.

and surprising because no single and double bond alternations take place in **5** in contrast to the other three structures. Although the structures **6** and **7** (Table 1) with C_s and D_{4h} symmetry of only 9 and 10 kcal/mol higher in energy, they do not correspond to local minima and instead they correspond to first-order transition states because each of them contains one imaginary frequency. Because of the estimated small differences in energy and in geometry, **6** and **7** can interconvert easily.

Next, the interaction of OTC with COT is considered. At first, to define the optimal spin state, we have examined the interaction of OTC with **5**. Because the ground-state electron configuration for the isolated osmium corresponds to $^5D_4$, two contrasting spin states for the combined complex were explicitly considered. The first is the quintet state structure **8** (Figure 5) with four unpaired electrons as in the case of isolated osmium atom, while the second structure **9** is at singlet ground state, where all electrons are mutually paired. B3LYP/SDD calculations have shown that **9** is energetically preferable as compared to **8**. Moreover, **8** is a higher order transition state structure because of the presence of two imaginary frequencies in frequency calculations. Since the possible move of OTC fragment in **9** from nearly the center of COT to any of its C═C double bond ends in an eight-member ring has an equal probability, it fails to explain the selectiveness in the shift observed experimentally. For this reason as well as taking into account the lowest stability of **5**, further calculations have been carried out only for interactions of OTC with **4**.

We have found that at the initial stage of interaction of OTC with **4**, complex **10** can be formed where the OTC group is slightly shifted from the center of COT to one of the C═C double bond ends because of nonsymmetrical orientations of the three carbonyl groups as compared to the two next-nearest C═C double bonds (Figure 6). At this orientation, the osmium atom of OTC establishes four Os−C bonds with C atoms of the eight-member ring at 2.228, 2.230, 2.464, and 2.465 Å, respectively. The frequency calculations have indeed confirmed that **10** corresponds to local minimum structure. The tub-shaped angle φ for the complex **10** is estimated to be 54°, an increase of about 15° from the value of the isolated structure **4**. Further shift of the OTC fragment in the direction of the nearest C═C double bond produces structure **11**, where the osmium atom of OTC establishes four new Os−C bonds with C atoms of the same ring at 2.267, 2.267, 2.355, and 2.355 Å, respectively (Figure 6). This structure **11** is 9.6 kcal mol^{-1} more stable than **10**. This shift of OTC group in **10** is the only direction that explains the formation of global minimum structure **11**. In **11**, the angle φ for the OTC-free part is estimated to be 7° showing a substantial decrease from the initial tub-shaped structure. At the same time, the other end-of-tube fragment coordinated to

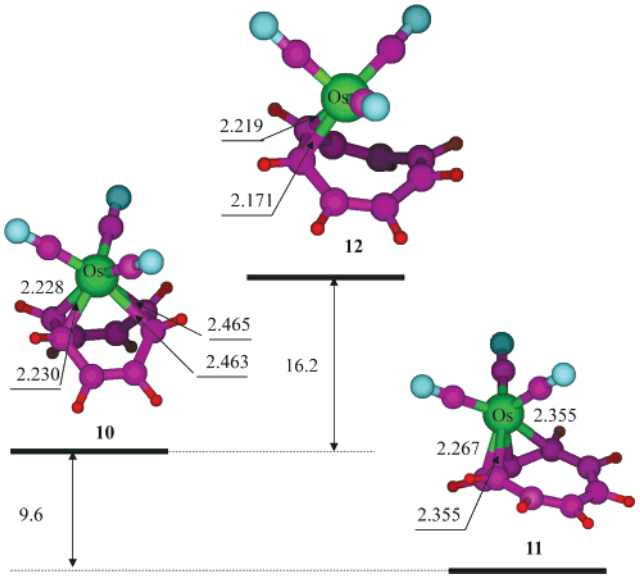

Figure 6. The optimized structures of TCO with **4** leading to the formation of (a) **10**, (b) **11**, and (c) **12**. The selected bond distances are in Å, energy differences are in kcal mol^{-1}.

OTC is only slightly increased (the angle $\varphi = 41.5°$). Thus, only one of the two tub-shaped ends of COT fragment establishes relatively coplanar orientation when complex **11** is formed (see Figure 6). The calculated chemical shifts for **11** support rather well the observed ones, especially for the ^{13}C chemical shifts, though they produce systematic overestimation of the experimental chemical shifts. For example, the predicted ^{13}C chemical shifts are equal to 59.3, 92.6, 125.1, and 130.7 ppm, respectively, at the distinct carbon atoms (cf. with Figure 1). To estimate the energy barrier necessary for this transformation from **10** to **11**, we have located the transition-state structure **12** (Figure 6) using the opt = qst3 option. It was found that the activation barrier for the transformation from **10** to **11** amounts to 16.2 kcal mol^{-1} (Figure 6). Frequency calculations have further confirmed that **12** is indeed the transition-state structure that has only one imaginary frequency (-190 cm^{-1}). In contrast to **10** and **11**, at transition-state **12**, the osmium atom has only two strong Os−C bonds with C atoms of the ring while the other two nearest Os−C bonds are strongly elongated and appeared at 2.844 and 3.322 Å, respectively.

Looking at the found structures from the point of view of the topology of haptotropic migrations in **3**, we conclude that the structure **11** corresponds to the ground state of **3**, whereas **10** and **12** correspond to the intermediate product and transition state connecting **10** and **11**, respectively. If, after the conversion of **11** to **10**, the reverse reaction would occur at another side of the molecule, the overall transformation would result in the [1,5]-Os haptotropic shift. Thus, our results demonstrate that the [1,5]-Os haptotropic migration is a stepwise process with quite high activation energy. This finding corresponds with another topology of the fast haptotropic migrations detected experimentally.

To mimic the experimentally observed [1,2]-M shift in **11**, additional calculations have been undertaken. Taking into account the degenerate nature of the initial and final products, we have located the transition-state structure **13** that explains the experimentally observed [1,2]-Os shift (Figure 7). The estimated activation energy barrier for the [1,2]-Os shift was equal to 6.5 kcal mol^{-1} in good agreement with the above experimental value (5.9 kcal mol^{-1}). Frequency calculations confirmed that **13** is indeed a transition-state structure with the

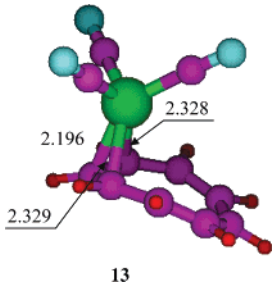

Figure 7. The optimized transition-state structure **13**. The selected bond distances are in Å.

only imaginary frequency appearing at -92 cm^{-1}. In contrast to **10**, **11**, and **12**, the osmium atom has only three strong Os−C bonds with C atoms of the ring at the transition-state **13** (Figure 7). Also, both ends of the COT fragment in **13** are bent in the direction opposite to the interacting OTC while the whole COT fragment can no longer be considered as a tub-shaped structure. Also, the predicted [1,2]-Os shift is the only rearrangement that proceeds with the lowest energy barrier. The other two rearrangements of (1,3) and (1,4) are both stepwise reactions, so that one should go first through the transition-state structure **12** to the intermediate structure **10** by overcoming the barrier of 25.8 kcal mol^{-1} and then obtains only the product of those distinct rearrangements.

Conclusions

In summary, we would like to underline that the theoretical calculations support well the [1,2]-M shift observed for **3**. The calculated activation energy barrier at the applied B3LYP/SDD level is extremely close to the experimentally observed one. The structure of the transition-state **13** implies that the [1,2]-Os shifts take place without considerable flattening of the COT cycle unlike the COT ring inversion. The flattened transition-state **12** is considerably higher in energy when compared to **13** and corresponds to a random migration of the organometallic group across the COT cycle. Nevertheless, the estimated transition-state structures **12** and **13** might be themselves of some importance in explaining the nature of bond-making/bond-breaking mechanisms in the haptotropic shifts of various transition-metal complexes.

References and Notes

(1) Woodward, R. B.; Hoffmann, R. *Angew. Chem.* **1969**, *81*, 797.

(2) (a) Gridnev, I. D.; Tok, O. L.; Gridneva, N. A.; Bubnov, Y. N.; Schreiner, P. R. *J. Am. Chem. Soc.* **1998**, *120*, 1034. (b) Gridnev, I. D.; Tok, O. L.; Gurskii, M. E.; Bubnov, Yu. N. *Chem. Eur. J.* **1996**, *2*, 1483.

(3) Cotton, F. A. *Acc. Chem. Res.* **1968**, *1*, 257.

(4) (a) Kreiter, C. G.; Maasbol, A.; Anet, F. A. L.; Kaesz, H. D.; Winstein, J. *J. Am. Chem. Soc.* **1966**, *88*, 3444. (b) Cotton, F. A.; Davison, A.; Faller, J. W. *J. Am. Chem. Soc.* **1966**, *88*, 4507. (c) Keller, C. E.; Shoulders, B. A.; Pettit, R. *J. Am. Chem. Soc.* **1966**, *88*, 4760. (d) Anet, F. A. L.; Kaesz, H. D.; Maasbol, A.; Winstein, S. *J. Am. Chem. Soc.* **1967**, *89*, 2489. (e) Anet, F. A. L. *J. Am. Chem. Soc.* **1967**, *89*, 2491.

(5) (a) Grubbs, R.; Breslow, R.; Herber, R.; Lippard, S. J. *J. Am. Chem. Soc.* **1967**, *89*, 6864. (b) Cotton, F. A.; Davison, A.; Musco, A. *J. Am. Chem. Soc.* **1967**, *89*, 6796; (c) Bratton, W. K.; Cotton, F. A.; Davison, A.; Musco, A.; Faller, J. W. *Proc. Natl. Acad. Sci. U.S.A.* **1967**, *58*, 1324. (d) Cotton, F. A.; Davidson, A.; Marks, T. J.; Musco, A. *J. Am. Chem. Soc.* **1969**, *91*, 6598. (e) Cotton, F. A.; Hunter, D. L. *J. Am. Chem. Soc.* **1976**, *98*, 1413.

(6) Cooke, M.; Goodfellow, R. J.; Green, M.; Maher, J. P.; Yandle, J. R. *Chem. Commun.* **1970**, 565.

(7) States, D. J.; Haberkorn, R. A.; Ruben, D. J. *J. Magn. Reson.* **1982**, *48*, 286.

(8) Perrin, C. L.; Dwyer, T. J. *Chem. Rev.* **1990**, *90*, 935.

(9) Cobas, J. C.; Martin-Pastor, M. EXSYCalc Version 1.0, MestReC 2004. The help file of this shareware contains full description of the

algorithm and important experimental aspects of quantitative EXSY. See also the web-site address http://www.mestrec.com/exsycalc.php.

(10) Kumar, A.; Wagner, G.; Ernst, R. R.; Wüthrich, K. *J. Am. Chem. Soc.* **1981**, *103*, 3654.

(11) (a) Becke, A. D. *Phys. Rev. A* **1988**, *38*, 3098. (b) Lee, C.; Yang, W.; Parr, R. G. *Phys. Rev. B* **1988**, *37*, 785.

(12) Frisch, M. J.; Trucks, G. W.; Schlegel, H. B.; Scuseria, G. E.; Robb, M. A.; Cheeseman, J. R.; Zakrzewski, V. G.; Montgomery, J. A., Jr.; Stratmann, R. E.; Burant, J. C.; Dapprich, S.; Millam, J. M.; Daniels, A. D.; Kudin, K. N.; Strain, M. C.; Farkas, O.; Tomasi, J.; Barone, V.; Cossi, M.; Cammi, R.; Mennucci, B.; Pomelli, C.; Adamo, C.; Clifford, S.; Ochterski, J.; Petersson, G. A.; Ayala, P. Y.; Cui, Q.; Morokuma, K.; Malick, D. K.; Rabuck, A. D.; Raghavachari, K.; Foresman, J. B.; Cioslowski, J.; Ortiz, J. V.; Stefanov, B. B.; Liu, G.; Liashenko, A.; Piskorz, P.; Komaromi, I.; Gomperts, R.; Martin, R. L.; Fox, D. J.; Keith, T.; Al-Laham, M. A.; Peng, C. Y.; Nanayakkara, A.; Gonzalez, C.; Challacombe, M.; Gill, P. M. W.; Johnson, B.; Chen, W.; Wong, M. W.; Andres, J. L.; Gonzalez, C.; Head-Gordon, M.; Replogle, E. S.; Pople, J. A. *GAUSSIAN 98*, Revision A.3; Gaussian Inc.: Pittsburgh, PA, 1998.

(13) Paik, D. H.; Yang, D.-S.; Lee, I.-R.; Zewail, A. H. *Angew. Chem., Int. Ed*. **2004**, *43*, 2830.

(14) Castano, O.; Palmeiro, R.; Frutos, L. M.; Luisandres, J. *J. Comput. Chem*. **2002**, *23*, 732.

(15) Miller, T. M.; Viggiano, A. A.; Miller, A. E. S. *J. Phys. Chem. A* **2002**, *106*, 10200.

(16) Frueholz, R. P.; Kuppermann, A. *J. Chem. Phys*. **1978**, *69*, 3614.